PROCEEDINGS OF SCIENCE

Parameter extractions for RHIC BES using Bayesian statistics

Jussi Auvinen*
Duke University / Institute of Physics Belgrade†
E-mail: jaa49@phy.duke.edu

Iurii Karpenko
INFN Florence / SUBATECH Nantes‡

Jonah E. Bernhard
Duke University

Steffen A. Bass
Duke University

We present the latest results on the collision energy dependence of η/s, obtained from a Bayesian model-to-data analysis of UrQMD + viscous hydrodynamics hybrid model to RHIC beam energy scan data for Au+Au collisions at 19.6, 39 and 62.4 GeV. Changes in the most likely value of η/s over beam energy scan range suggest a dependence on baryon chemical potential μ_B. However, we also find the uncertainties regarding the value of η/s to be notable at $\sqrt{s_{NN}} = 19.6$ GeV.

Critical Point and Onset of Deconfinement
7-11 August, 2017
The Wang Center, Stony Brook University, Stony Brook, NY

*Speaker.
†Current affiliation.
‡Current affiliation.

PoS(CPOD2017)019

1. Introduction

Experiments at RHIC and LHC are presently focused on quantifying the transport properties of the quark-gluon plasma (QGP) and mapping out the QCD phase diagram. As the transition between QGP and hadronic matter is known to be a cross-over at top RHIC energies and at LHC, the beam energy scan (BES) program at RHIC investigates signals of a possible critical point – indicating the change to a first-order phase transition – at lower collision energies, where the QCD matter is exposed to typically lower temperatures but higher net-baryon densities.

The beam energy scan presents multiple challenges to theoretical models of relativistic heavy ion collisions. The initial non-equilibrium evolution of the system becomes more prominent and can have a large effect on the outcome of the calculations. Moreover, a full (3+1)-D hydrodynamical model is required to describe the evolution of the medium, as the simplifying assumption of a midrapidity plateau is no longer valid. In addition, the non-zero baryon chemical potential μ_B needs to be taken into account in the equation of state. These challenges can be overcome using a hybrid approach, where the the non-equilibrium evolution of the system is described with a microscopic hadronic transport model, while a (3+1)-D viscous hydrodynamics model is utilized to model the system close to thermal equilibrium.

Due to the complex nature of the problem, the models of heavy ion collisions at BES range typically have numerous parameters, each of them contributing to final results of multiple physical observables in the model calculations. Thus the most robust approach for tuning a model would be to simultaneously fit all model parameters to all available experimental data. However, after finding a combination of input parameters which gives a good description of the data, the question then becomes how many other combinations would produce an equally good description, and how much each individual parameter is allowed to vary within this set of equally good parameter combinations.

This problem of multidimensional parameter fitting and the related uncertainty estimation can be addressed using the framework of Bayesian statistics, which has already been very successfully applied to $Au+Au$ collisions at the top RHIC energy and $Pb+Pb$ collisions at the LHC [1, 2, 3]. The outcome of the Bayesian analysis is a multidimensional probability distribution for all the input parameter combinations of the investigated model. Based on this probability distribution, we can make statements about what parameter values are most likely to provide a good description of the experimental data, and how large uncertainties we should associate to any given parameter values.

In this proceedings article, we apply Bayesian analysis on the input parameters of a transport + (3+1)-D viscous hydrodynamics model [4] to investigate the μ_B dependence of η/s in $Au+Au$ collisions, using the collision energy $\sqrt{s_{NN}}$ as the control parameter with values 19.6, 39.0, and 62.4 GeV. We give a brief description of the hybrid model in Section 2. The Bayesian analysis methods are described in Section 3 and the results of the analysis are presented in Section 4. A summary of the investigation is provided in Section 5.

2. Transport + hydrodynamics hybrid model

In the hybrid model used for this study [4], the time evolution of the collision system is simulated in three separate phases. The UrQMD hadron-string cascade [5, 6] is used for the initial

non-equilibrium evolution. The duration of the initial phase is controlled with the time parameter τ_0, which is constrained from below by the condition that the two colliding nuclei must have passed through each other during this phase.

At the time $\tau = \tau_0$, the microscopic particle properties are mapped to hydrodynamic densities using 3-D Gaussians with width parameters $W_{\rm trans}$, $W_{\rm long}$. These density profiles provide the initial state for the hydrodynamical evolution, which is done using a (3+1)-D relativistic viscous hydrodynamics code [7]. The shear viscosity of the medium is adjusted with the input parameter η/s, which is treated as a constant throughout the hydrodynamical phase. A chiral model equation of state [8] is used to accommodate for finite values of baryon chemical potential.

Finally, the energy density parameter ε_{SW} is used to govern the transition from hydrodynamics back to UrQMD for final scatterings and decays. Once the local rest frame energy density in all hydro cells has fallen below ε_{SW}, hadrons to be evolved in the final phase are sampled according to Cooper-Frye procedure from the iso-energy density hypersurface $\varepsilon(t,x) = \varepsilon_{SW}$. The hypersurface is constructed by the Cornelius hypersurface finder [9].

3. Statistical analysis

The Bayes' theorem states that the posterior probability for a combination of input parameters $\vec{x} = (\eta/s, \tau_0, W_{\rm trans}, W_{\rm long}, \varepsilon_{SW})$ to provide the best description of the data is a product of our prior knowledge $P(\vec{x})$ about the plausible range of values for each parameter, and the likelihood $\mathscr{L}(\vec{x})$ of the given combination of parameter values when compared to experimental data. For the present study, the prior probability $P(\vec{x})$ distribution is a uniform 5-dimensional box, while the likelihood function has the general form

$$\mathscr{L}(\vec{x}) \propto \exp\left(-\frac{1}{2}(\vec{y}(\vec{x}) - \vec{y}^{\rm exp})^T \Sigma^{-1}(\vec{x})(\vec{y}(\vec{x}) - \vec{y}^{\rm exp})\right) \tag{3.1}$$

where the covariance Σ matrix contains the uncertainties associated with the comparison of model output $\vec{y}(\vec{x})$ and the experimental data $\vec{y}^{\rm exp}$; more precisely, Σ includes statistical and systematic errors (summed in quadrature) and the emulator error (described below).

We sample the Bayesian posterior distribution using Markov chain Monte Carlo (MCMC), where the starting points of the random walkers are taken from the prior $P(\vec{x})$, while the probability for a walker to accept a proposed step direction is determined by the likelihood function $\mathscr{L}(\vec{x})$.

As the MCMC sampling involves $\mathscr{O}(10^3)$ random walkers performing $\mathscr{O}(10^4)$ steps, fast evaluation of the likelihood function becomes necessary. Clearly running full hybrid model simulations to determine $\vec{y}(\vec{x})$ for an arbitrary $\vec{x}$ requires an infeasible amount of computational effort in this context. The solution to this problem is to use a surrogate model, namely a Gaussian process (GP) emulator [10], to estimate $\vec{y}(\vec{x})$. In addition to predicting the model output, GP emulators provide also uncertainty estimation by construction, which is included in the covariance matrix in the likelihood computation.

GP emulators need to be conditioned on training data to make sensible predictions. We have sampled ~ 100 training points for each collision energy, using Latin hypercube method to distribute the points evenly in the input parameter space.

4. Results

To impose strong constraints on the model parameters, our aim has been to use as comprehensive set of experimental data as possible for each collision energy. For $\sqrt{s_{NN}} = 62.4$ GeV, we have included charged particle multiplicities $N_{\rm ch}$ [11], pseudorapidity distributions $dN_{\rm ch}/d\eta$ [12], and elliptic flow $v_2\{\rm EP\}$ [13, 14]. Identified particle observables include charged pion HBT radii $R_{\rm out}$, $R_{\rm side}$ and $R_{\rm long}$ [15], the multiplicity ratio of K^+ and π^+ and their mean transverse momenta [11], as well as the multiplicity and $\langle p_T \rangle$ of Ω [16, 17]. At $\sqrt{s_{NN}} = 39$ GeV, the available data consists of charged particle elliptic flow $v_2\{2\}$ [13], charged pion HBT radii, multiplicities and mean transverse momentum of π^+, π^-, K^+ and K^- [18], as well as the p_T spectrum of Ω [19]. In addition to the observables at 39 GeV, the data set at $\sqrt{s_{NN}} = 19.6$ GeV includes also the charged particle pseudorapidity distribution [12].

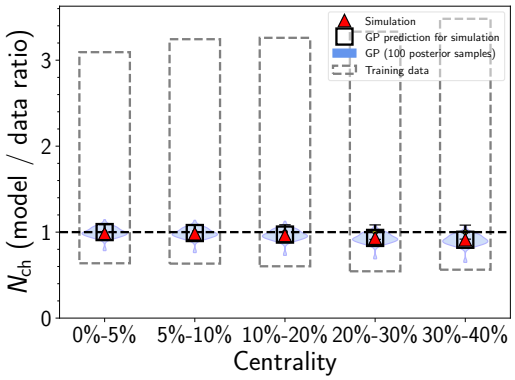

Figure 1: Model-to-data ratio of charged particle multiplicity for five centrality classes at $\sqrt{s_{NN}} = 62.4$ GeV. Grey dashed boxes represent the initial range of values from the training data, while the widths of the blue shaded areas illustrate the probability densities for expected outcomes using samples from the posterior distribution. Red triangles show the result from full hybrid model simulations using the median values of the posterior distribution for the input parameters, and open squares indicate the emulator predictions for the median value simulations.

An example of the effectiveness of the statistical analysis procedure is demonstrated in figure 1. The initial results from the emulator training points allow for multiplicities over three times larger than the measured values. After the model-to-data calibration procedure, the range of multiplicities has shrunk within 10% of the measurement for the majority of the input parameter combinations sampled from the posterior distribution. There is a trend for underestimating $N_{\rm ch}$ at more non-central collisions; this may indicate that using the same value of τ_0 for all centralities is an oversimplification and a more sophisticated initial state model with an impact parameter dependent τ_0 is needed.

The emulator prediction quality is also demonstrated in Fig. 1 by showing both the full hybrid model simulations, where the median values of the posterior probability distributions were used as the input parameters, and the respective emulator predictions for the same parameter values. As seen in the figure, the predictions are very accurate for all centralities.

Figure 2 shows one-dimensional projections of the posterior probability distributions for shear viscosity over entropy density ratio η/s and hydro-to-transport switching energy density ε_{SW} for

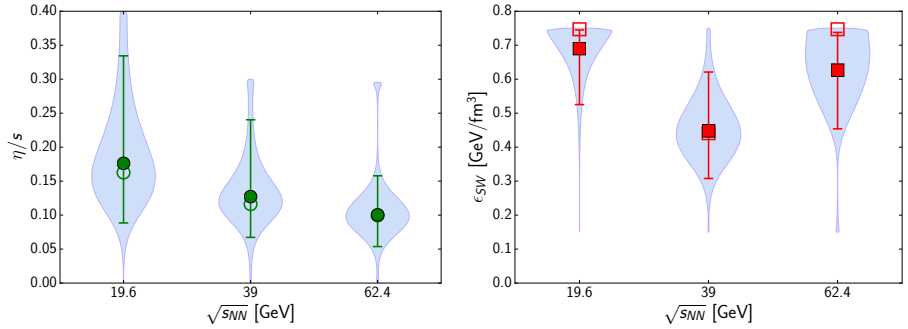

Figure 2: Violin plots of the collision energy dependence of 1-D posterior probability distributions of shear viscosity over entropy density η/s (left) and hydro-to-transport switching energy density ε_{SW} (right). Open symbols indicate the peak values of the distributions, while the full symbols and associated error bars represent median values and 90% confidence limits, respectively. For each plot, the width of the shaded area reflects the probability density at the corresponding parameter value.

the three investigated collision energies. The most probable value of η/s increases towards lower collision energies, but the same is true also for the uncertainties. At present there remains a significant probability density overlap in the range $\eta/s = 0.10 - 0.15$, so a constant value within that range remains a possibility.

The switching energy density does not have an obvious trend with respect to the collision energy. Wide probability distributions at 39 GeV and 62.4 GeV are consistent with the underlying assumption of a range of density values where hydrodynamics and hadron transport provide an equal description of the system. However, a very early transition from hydrodynamical evolution to hadron transport is preferred at $\sqrt{s_{NN}} = 19.6$ GeV.

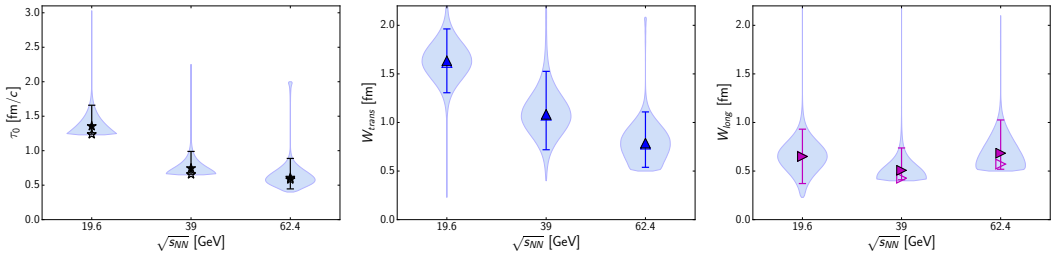

Figure 3: Violin plots of the collision energy dependence of 1-D posterior probability distributions of hydro starting time τ_0 (left), transverse smearing parameter W_{trans} (center), and switching energy density W_{long} (right).

We present an illustration of the collision energy dependencies of the posterior distributions of the initial state parameters in figure 3. As mentioned in section 2, the hydro starting time τ_0 is limited from below by the interpenetration time of the two colliding nuclei, which is longer at lower collision energies. Overall, the earliest possible starting time for hydrodynamics is preferred at all three collision energies.

The two initial density profile smearing parameters have notably different collision energy dependencies. While the most likely value for the longitudinal smearing parameter W_{long} remains roughly constant over the investigated energy range, the amount of transverse profile smearing

needed for the best description of the experimental data is much larger at $\sqrt{s_{NN}} = 19.6$ GeV compared to 62.4 GeV.

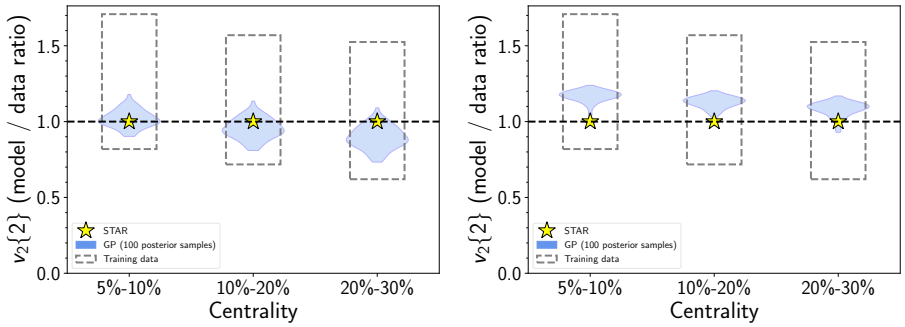

Figure 4: Model-to-data ratio of charged particle elliptic flow $v_2\{2\}$ for three centrality classes at $\sqrt{s_{NN}} =$ 19.6 GeV. Left: Samples from the full posterior distribution. Right: Samples from the posterior distribution limited to $W_{\mathrm{trans}} \leq 1.0$ fm (the narrow tail of W_{trans} in the middle panel of figure 3).

The relatively high peak value of ε_{SW} and the increase in the hydro starting time τ_0 work to diminish the role of hydrodynamics on the time evolution of the collision system at $\sqrt{s_{NN}} = 19.6$ GeV. At the same time the large values of η/s and W_{trans} are expected to further decrease elliptic flow and increase the final particle multiplicity [4]. Indeed, as shown in figure 4, the smaller values of W_{trans} cause $v_2\{2\}$ predictions to be systematically above data.

5. Summary

We have utilized Bayesian statistics combined with Gaussian process emulators for a robust and comprehensive model-to-data comparison on a transport + hydrodynamics hybrid model describing $Au+Au$ collisions at RHIC beam energy scan. We find the most likely value of shear viscosity over entropy density ratio to be largest at $\sqrt{s_{NN}} = 19.6$ GeV and smallest at $\sqrt{s_{NN}} = 62.4$ GeV, suggesting that η/s depends on baryon chemical potential μ_B. A constant value of η/s cannot be fully excluded with the present uncertainties, however.

6. Acknowledgements

This work has been supported by NSF grant no. NSF-ACI-1550225 and by DOE grant no. DE-FG02-05ER41367. I. K. acknowledges partial support by the University of Florence grant *Fisica dei plasmi relativistici: teoria e applicazioni moderne*. CPU time was provided by the Open Science Grid, supported by DOE and NSF.

References

[1] S. Pratt, E. Sangaline, P. Sorensen and H. Wang, Phys. Rev. Lett. **114** (2015) 202301 [arXiv:1501.04042 [nucl-th]].

[2] J. E. Bernhard, J. S. Moreland, S. A. Bass, J. Liu and U. Heinz, Phys. Rev. C **94**, no. 2 (2016) 024907 [arXiv:1605.03954 [nucl-th]].

[3] J. F. Paquet, C. Shen, G. Denicol, S. Jeon and C. Gale, Nucl. Phys. A **967** (2017) 429.

[4] I. A. Karpenko, P. Huovinen, H. Petersen and M. Bleicher, Phys. Rev. C **91**, no. 6 (2015) 064901 [arXiv:1502.01978 [nucl-th]].

[5] S. A. Bass *et al.*, Prog. Part. Nucl. Phys. **41** (1998) 255 [nucl-th/9803035].

[6] M. Bleicher *et al.*, J. Phys. G **25** (1999) 1859 [hep-ph/9909407].

[7] I. Karpenko, P. Huovinen and M. Bleicher, Comput. Phys. Commun. **185** (2014) 3016 [arXiv:1312.4160 [nucl-th]].

[8] J. Steinheimer, S. Schramm and H. Stocker, J. Phys. G **38** (2011) 035001 [arXiv:1009.5239 [hep-ph]].

[9] P. Huovinen and H. Petersen, Eur. Phys. J. A **48** (2012) 171 [arXiv:1206.3371 [nucl-th]].

[10] C. E. Rasmussen and C. K. I. Williams, *Gaussian Processes for Machine Learning*, The MIT Press, Cambridge, MA 2006.

[11] B. I. Abelev *et al.* [STAR Collaboration], Phys. Rev. C **79** (2009) 034909 [arXiv:0808.2041 [nucl-ex]].

[12] B. Alver *et al.* [PHOBOS Collaboration], Phys. Rev. C **83** (2011) 024913 [arXiv:1011.1940 [nucl-ex]].

[13] L. Adamczyk *et al.* [STAR Collaboration], Phys. Rev. C **86** (2012) 054908 [arXiv:1206.5528 [nucl-ex]].

[14] N. Magdy [STAR Collaboration], J. Phys. Conf. Ser. **779**, no. 1 (2017) 012060.

[15] L. Adamczyk *et al.* [STAR Collaboration], Phys. Rev. C **92**, no. 1 (2015) 014904 [arXiv:1403.4972 [nucl-ex]].

[16] M. M. Aggarwal *et al.* [STAR Collaboration], Phys. Rev. C **83** (2011) 024901 [arXiv:1010.0142 [nucl-ex]].

[17] S. Chatterjee, S. Das, L. Kumar, D. Mishra, B. Mohanty, R. Sahoo and N. Sharma, Adv. High Energy Phys. **2015** (2015) 349013.

[18] L. Adamczyk *et al.* [STAR Collaboration], Phys. Rev. C **96**, no. 4 (2017) 044904 [arXiv:1701.07065 [nucl-ex]].

[19] L. Adamczyk *et al.* [STAR Collaboration], Phys. Rev. C **93**, no. 2 (2016) 021903 [arXiv:1506.07605 [nucl-ex]].